Synthesis and Structure-Affinity Relationship of Small Molecules for Imaging Human CD80 by Positron Emission Tomography

Journal Article

Author(s):
Taddio, Marco F.; Mu, Linjing (iD); Castro Jaramillo, Claudia Adriana (iD); Bollmann, Tanja; Schmid, Dominik M.; Muskalla, Lukas P.; Gruene, Tim; Chiotellis, Aristeidis; Ametamey, Simon M.; Schibli, Roger; Krämer, Stefanie D.

SYNTHESIS AND STRUCTURE AFFINITY RELATIONSHIP OF SMALL MOLECULES FOR IMAGING HUMAN CD80 BY POSITRON EMISSION TOMOGRAPHY

Marco F. Taddio[1], Linjing Mu[1,2], Claudia A. Castro Jaramillo[1], Tanja Bollmann[1], Dominik Schmid[1], Lukas Muskalla[3], Tim Grüne[3,4], Aristeidis Chiotellis[1], Simon M. Ametamey[1], Roger Schibli[1], Stefanie D. Krämer[1*]*

[1] Center for Radiopharmaceutical Sciences ETH, PSI and USZ, Department of Chemistry and Applied Biosciences, ETH Zurich, CH-8093 Zurich, Switzerland; [2] Department of Nuclear Medicine, University Hospital Zurich, CH-8091 Zurich, Switzerland; [3] Laboratory for Catalysis and Sustainable Chemistry, Paul Scherrer Institute, CH-5232 Villigen PSI, Switzerland; [4] X-ray Structure Analysis Centre, Faculty of Chemistry, University of Vienna, A-1090 Vienna, Austria

Abstract

The co-stimulatory molecule CD80 is an early marker for immune activation. It is upregulated on activated antigen-presenting cells. We aimed at developing a tracer for imaging CD80 by positron emission tomography (PET). Novel CD80 ligands were synthesized and tested by SPR for affinity to human CD80 (hCD80) and displacement of endogenous ligands. Several compounds bound with one-digit nanomolar affinity to hCD80 and displaced CTLA-4 and CD28 at nanomolar concentrations. A structure-affinity relationship study revealed relevant moieties for strong affinity to hCD80 and positions for further modifications. Lead compound MT107 (**7f**) was radiolabelled with carbon-11. *In vitro*, [^{11}C]MT107 showed specific binding to hCD80-positive tissue and high plasma protein binding. *In vivo*, [^{11}C]MT107 accumulated in liver, gall bladder and intestines, but only scarcely in hCD80-positive xenografts. The unfavourable *in vivo* performance may result from high plasma protein binding and extensive biliary excretion.

ABSTRACT

The co-stimulatory molecule CD80 is an early marker for immune activation. It is upregulated on activated antigen-presenting cells. We aimed at developing a tracer for imaging CD80 by positron emission tomography (PET). Novel CD80 ligands were synthesized and tested by SPR for affinity to human CD80 (hCD80) and displacement of endogenous ligands. Several compounds bound with one-digit nanomolar affinity to hCD80 and displaced CTLA-4 and CD28 at nanomolar concentrations. A structure-affinity relationship study revealed relevant moieties for strong affinity to hCD80 and positions for further modifications. Lead compound MT107 (**7f**) was radiolabelled with carbon-11. *In vitro*, [^{11}C]MT107 showed specific binding to hCD80-positive tissue and high plasma protein binding. *In vivo*, [^{11}C]MT107 accumulated in liver, gall bladder and intestines, but only scarcely in hCD80-positive xenografts. The unfavourable *in vivo* performance may result from high plasma protein binding and extensive biliary excretion.

INTRODUCTION

The co-stimulatory molecules CD80 (B7-1) and CD86 (B7-2) are expressed on activated antigen-presenting cells. They interact with immune-modulatory molecules on T cells, among them CTLA-4 and CD28. The weak-affinity interaction of CD80 or CD86 with CD28 is involved in T-cell activation, while the strong interaction of CD80/CD86 with CTLA-4 prevents T-cell activation.[1,2,3] The balance between T cell activation and inactivation is disturbed in various diseases including cancer[4], atherosclerosis[5,6], autoimmune diseases[7] and transplant rejection[8]. Several therapeutic strategies aim at modulating the levels or functions of the co-stimulatory molecules accordingly. CD80/CD86 and their receptors are targeted by immunotherapies for various indications.[9,10] However, following their dual functionality, finding the right balance in CD80/CD86 modulation remains challenging. Diagnosis, disease staging and therapy planning may benefit from a non-invasive method to detect and quantify T-cell activating co-stimulatory molecules in tissue.

Several fusion proteins are on the market which bind to CD80 and CD86 with strong affinity leading to co-stimulation blockade and anergy of T cells. Abatacept and belatacept are successfully used in rheumatoid arthritis[9,10] and for the prophylaxis of organ rejection in transplantation medicine, respectively.[11,12] Both are fusion proteins of the extracellular domain of CTLA-4 and the IgG Fc part. Belatacept contains two pointmutations in the binding domains which result in a 2-fold stronger affinity to human CD80 and a 4-fold stronger affinity to human CD86 as compared to abatacept.[11]

Low molecular weight compounds with strong affinities to CD80 were developed to overcome the drawback of negligible oral bioavailability of the fusion proteins.[13,14,15,16] Erbe *et al.* discovered a binding site for small molecules on human CD80 (hCD80) which is adjacent to the binding domains for CTLA-4 and CD28, respectively.[13] The small-molecule binding site is absent on

rodent CD80 as concluded from both the amino acid sequence and absence of strong-affinity binding of the low molecular weight ligands of hCD80.[13] In the year 2004, Huxley *et al*. published structures with strong affinities and high selectivity for hCD80 over hCD86.[15]

Previous work from our group with a carbon-11 labelled radiotracer ([¹¹C]AM7), based on the lead structure from Huxley *et al*.[15] (**1** in Fig. 1), showed promising results in *in vitro* autoradiography experiments with hCD80-positive xenograft and human atherosclerotic plaque tissue slices. However, it had unfavourable pharmacokinetic properties in mice with high plasma protein binding (human and mouse) and substantial biliary excretion. *In vivo* accumulation in a hCD80-positive xenograft was poor.[6]

In this study, we explored the potential of structurally modified CD80 ligands for the development of a PET tracer with altered pharmacokinetics. We increased the structural diversity by hybridisation of the lead structures introduced by Huxley *et al*.[15] and Green *et al*.[14] and investigated the structure-affinity relationship of the new compounds by surface plasmon resonance (SPR). A ligand combining core-structure modifications and strong affinity was labelled with carbon-11 and evaluated by PET/CT in mice with hCD80-positive Raji xenografts.

RESULTS

Chemistry. A cinnoline-based compound (**1**)[15] and pyrazolopyridine-based compounds (**2, 3**)[14]

were previously reported as potent small molecule ligands for hCD80. Based on these core

structures, we designed and synthesized novel cinnoline-, quinoline- and pyrazolopyridine-based

compounds in this work. Replacement of the methyl-pyrazole moiety of compound **2** with the

benzene ring of compound **1** led to novel quinoline-based compounds **7e-g** (Figure 1). The acid

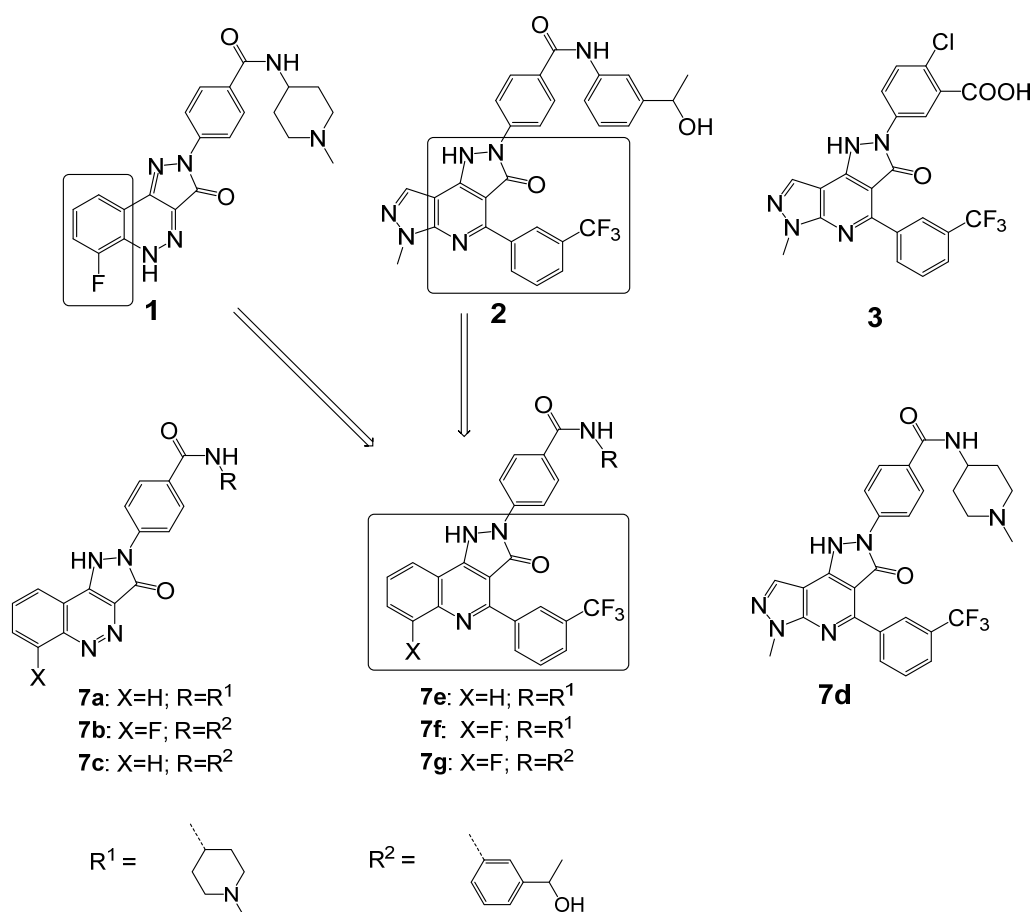intermediates were included for comparison with the acid compound **3**.

Figure 1. Structures of the synthesized compounds. Boxes indicate structural features from reported compounds (**1** & **2**) which were conserved in hybrid compounds **7e – 7g**.

Three series of cinnoline-, quinoline- and pyrazolopyridine-based compounds were synthesized based on the modified synthetic procedures as previously described.[14,15] Scheme 1 depicts the synthetic route for cinnoline-based compounds. Compounds **5a** and **5b** were synthesized by reacting their corresponding phenylhydrazonomalonic acid with thionylchloride, cyclization and methyl ester formation in the presence of TiCl$_4$ and methanol. Converting the hydroxyl group to the chlorinated intermediate, then reacting with 4-hydrazino-benzoic acid formed the key acid compounds **6a** and **6b** in more than 75% yields. Subsequently, coupling with 1-methylpiperidin-4-amine or 1-(3-aminophenyl)ethan-1-ol afforded compounds **1** and **7a-c** in moderate yields.
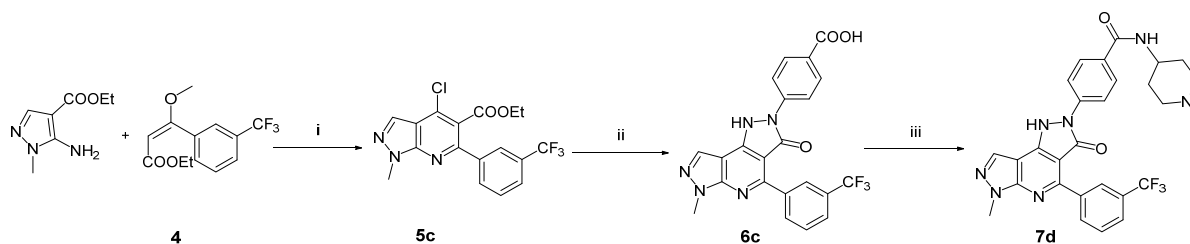
Scheme 1: Synthetic pathway towards cinnoline-based compounds.
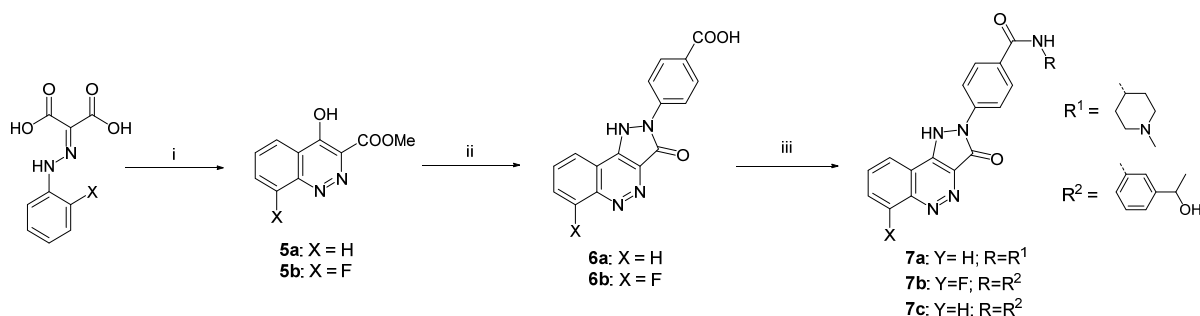
Reagents and conditions: (i) 1) SOCl$_2$, 80°C; 2) TiCl$_4$, 110°C; 3) MeOH, 60°C; (ii) 1) SOCl$_2$, 80°C, 1 h; 2) 4-hydrazinylbenzoic acid, 70°C, EtOH, 1 h; (iii) R-NH$_2$, EDC, DIPEA, rt, DMF, 18 h. R^1, R^2, see Figure 1.

The pyrazolopyridine- and quinoline-based compounds were synthesized as illustrated in Scheme 2 and 3, respectively. Compound **4** was synthesized by heating ethyl 3-(trifluoromethyl)benzoate in EtOAc with sodium hydride and subsequent methylation with trimethylsilyldiazomethane at room temperature with 48% yield. Gould-Jacobs cyclisation with ethyl 3-methoxy-3-(3-(trifluoromethyl)phenyl)acrylate (**4**) under strong basic conditions, followed by substitution of the hydroxy group by chlorine using phosphorous oxychloride, afforded 1-methyl-1*H*-pyrazolo[3,4-b]pyridine (**5c**) or quinolines (**5d**, **5e**) with 55-61% yields. Subsequent Knorr pyrazole ring formation with hydrazinyl benzoic acid derivatives under basic conditions and heating afforded compounds **6c-e** in 66-85% and compound **3** in 31% yield. In the last step, the carboxylic acid was activated with a coupling reagent (EDC hydrochloride or HATU) and two different building blocks (*meta*-1-hydroxyethyl-phenyl or *para*-1-methylpiperidinyl) were introduced by amide bond formation in 13-87% yields (**2, 7d-g**).

Scheme 2: Synthetic route for pyrazolopyridine-based compound **7d**.

Reagents and conditions: (i) 1) NaH, reflux, THF, 16 h; 2) POCl3, 120°C, 2 h; (ii) 4-hydrazinylbenzoic acid, NaOtBu, 100°C, ethylene glycol, 18 h; (iii) 1-methylpiperidin-4-amine, EDC, DIPEA, rt, DMF, 18 h

Scheme 3: Synthetic pathway toward quinoline-based compounds.
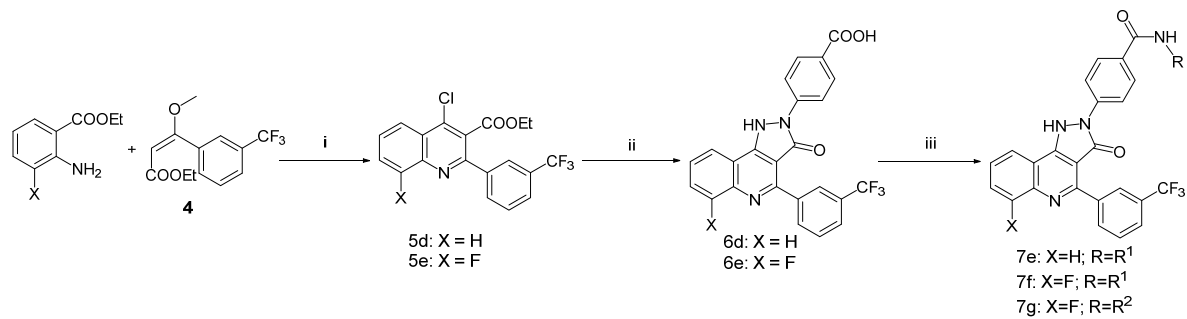
Reagents and conditions: (i) 1) NaH, reflux, THF, 16 h; 2) POCl$_3$, 120°C, 2 h; (ii) 4-hydrazinylbenzoic acid, NaO^{t}Bu, 100°C, ethylene glycol, 18 h; (iii) R-NH$_2$, HATU, DIPEA, rt, DMF, 30 min. R^1, R^2, see Figure 1.

Table 1: Synthesized compounds (structures and substituents according to Figure 1 and Scheme 1) and their affinity to hCD80 determined by surface plasmon resonance.

Compound	X	R	$K_d \pm SD$ [nM] (n)
1 (AM7)	F	R^1	3.8 ± 2.5 (*9*)
2	-	R^2	142 ± 61 (*3*)
3	-	-	90.7, 48.4 (*2*)
6a	H	-	572, 368 (*2*)
6b	F	-	n.d.
6c	-	-	308, 397 (*2*)
6d	H	-	194 (*1*)
6e	F	-	n.d.
7a	H	R^1	9.3, 10.7 (*2*)
7b	F	R^2	120, 72 (*2*)
7c	H	R^2	117, 310 (*2*)
7d	-	R^1	109 ± 10 (*3*)
7e	H	R^1	7.1, 6.5 (*2*)
7f (MT107)	F	R^1	4.2 ± 2.3 (*9*)
7g	F	R^2	113 ± 50 (*4*)

(*n*), number of experiments; SD, standard deviation; n.d., not determined. K_d values of individual experiments are shown for n ≤ 2. R^1, R^2, see Figure 1.

Binding to hCD80. After the synthesis of the unlabelled compounds in Table 1, we investigated their affinity and kinetics for the binding to recombinant hCD80 (rhCD80) by SPR. Typical binding curves are shown in Supplementary Figure S1. The calculated binding rate constant (k_{on}) ranged from 9×10^4 to 7×10^5 $M^{-1}s^{-1}$. The dissociation rate constant (k_{off}) ranged from 4×10^{-4} to 0.4 s^{-1} and K_d from 3.8 to 572 nM (Table 1). In order to reach high signal ratios between hCD80-positive and negative tissues in PET imaging, we aimed at a strong affinity (low K_d) with a low k_{off}. This is the case for compounds in the right upper corner in the plot $1/K_d$ *vs* $1/k_{off}$ in Figure 2 (**1**, **7a**, **7e**, **7f**).
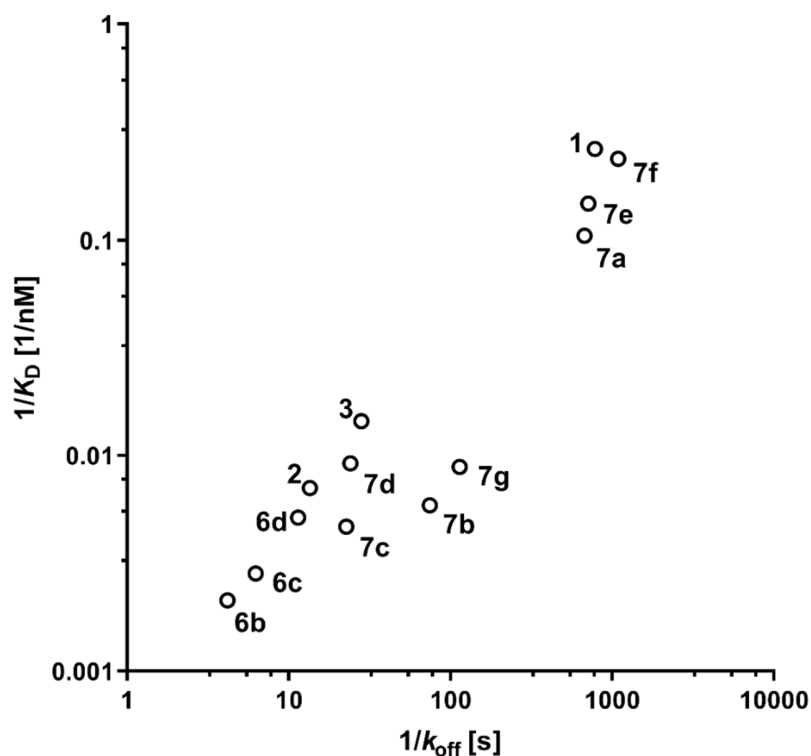
Figure 2. $1/K_d$ plotted against $1/k_{off}$ from SPR experiments. Compounds with preferred binding properties for PET imaging are in the upper right corner (low K_d, low k_{off}).

Displacement of hCTLA-4 and hCD28 from hCD80 binding. We next investigated by SPR the potential of **1, 2** and **7f** for displacing the binding domains of hCTLA-4 (in our study abatacept) and rhCD28 from the binding to rhCD80. We first confirmed published K_d values of rhCTLA-4 (0.27 nM) and rhCD28 (16.3 nM) to rhCD80.[17] In our assay, they were 0.5 nM and 17.8 nM, respectively ($n = 1$). For the displacement assay, we used abatacept and rhCD28 at concentrations 3-4-fold above their K_d values, $i.e.$, 2 nM and 50 nM, respectively. According to the Cheng-Prusoff equation, keeping a constant ratio between concentration and K_D of a displaced ligand (abatacept) should result in similar IC_{50} values for a particular displacer compound in varying experiments.

The displacement of abatacept was most effective by **1** and **7f** with IC_{50} values around 15 nM (Figure 3). The IC_{50} was more than one magnitude higher for **2**. The IC_{50} values for the displacement of rhCD28 were around 10 nM for **1** and **7f**, as shown in Figure 3 (not determined for **2**). The respective K_i values calculated from these data are shown in Figure 3. The K_i determined in the displacement experiments were in agreement with the K_d values determined in the direct binding experiments (Table 1). Furthermore, **7f** competed only weakly (at concentrations > 50 µM) with the binding of abatacept to rhCD86 and recombinant murine CD80 (rmCD80), in agreement with its selectivity for hCD80 over hCD86 and mCD80 (Supplementary Figures S2 and S3).
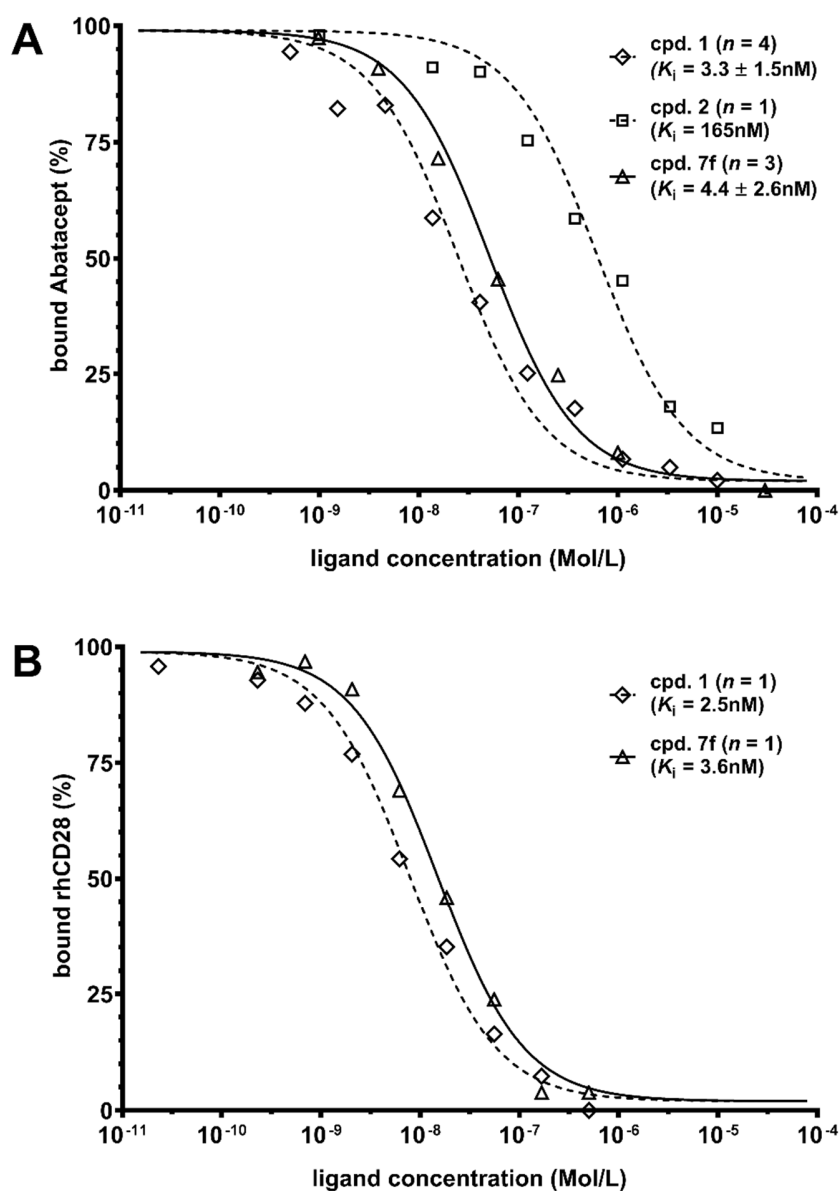
Figure 3: Representative displacement curves of (**A**) 2 nM abatacept or (**B**) 50 nM rhCD28 from immobilized rhCD80 by small molecules **1**, **2** (only in **A**) or **7f**. IC_{50} values were determined from the displacement by different concentrations of synthesized small molecules (x axis) assuming 1:1 binding stoichiometries. The respective (averaged) K_i values ($\pm$ S.D. for $n \geq 3$) are indicated in the Figure. n, number of experiments for K_i determination.

Radiosynthesis of [^{11}C]1 and [^{11}C]7f. Precursor compounds for radiolabelling were synthesized from intermediates **6b** and **6e** (shown in Scheme 1 and 3, respectively). By activation of the carboxylic acid with the coupling reagent EDC and following amide bond formation 1-boc-piperidin-4-amine under basic conditions, a boc-protected piperidine was introduced which was subsequently deprotected with DCM/TFA to afford compounds **8a** and **8b** in good yields (details in experimental section). Our group recently described the radiolabelling procedure of **1** with carbon-11 (ref. 6). This procedure was applied for the radiosynthesis of both [^{11}C]1 and our new radiotracer [^{11}C]7f. Details on the one-step radiosynthesis are described in the experimental section. Molar activities at the end of synthesis were between 200 and 500 GBq/μmol for [^{11}C]1 and between 20 and 80 GBq/μmol for [^{11}C]7f.

Lipophilicity, membrane permeability & plasma protein binding. *In vivo*, [^{11}C]1 scarcely distributed to the tissue, in agreement with its low log D at pH 7.4 of 0.1 and its low free fraction in plasma of 0.02.[6] We determined log D of [^{11}C]7f at various pH. **7f** differs from **1** by the C-[3-(trifluoromethyl)phenyl] moiety replacing the nitrogen in position 2 of the cinnoline substructure (Figure 1 and Table 1). As expected, this modification rendered the compound more lipophilic, with a log D at pH 7.4 of 1.98 ± 0.06. The log D was significantly lower at pH 5.4 than at higher pH values (Supplementary Figure S4). This is in agreement with the distribution characteristics of a basic compound (tertiary amine in R^2, Figure 1). The fit log P was 2.1 with a fit pK_a of 7.1.

We furthermore investigated the potential of the synthetized compounds **1**, **2**, **7e**, **7f** and **7g** to cross lipid bilayers at pH 7.4, using a recently introduced liposomal fluorescent permeability assay.[18]

The logarithmic permeability coefficients, log (P_{FLipP}, cm/s), ranged from -6.7 to -5.4, indicating poor to moderate membrane permeability.[18] Permeation kinetics were fastest for **1**, **7e** and **7f** with log P_{FLipP} above -6.

The plasma protein binding of [11C]**7f** was investigated with human plasma and bovine serum albumin (BSA) using ultracentrifugation filter units. The free fraction was 0.023 ± 0.002 ($n = 4$) for human plasma which is similar to the plasma protein binding of [11C]**1**[6], and a higher free fraction for BSA of 0.159 ± 0.002 ($n = 3$).

In vitro autoradiography. We chose compound **7f** for further *in vitro* and *in vivo* evaluation based on its strong binding affinity to hCD80 (low K_d) at low k_{off} (Figure 2 and Supplementary Figure S1) and as it differed from **1** in at least one physicochemical property (higher lipophilicity). Structural modifications with higher predicted impact on the physicochemical properties (*e.g.*, protonation/deprotonation equilibria) resulted in weakened binding affinity (Figures 1, 2 and Table 1). *In vitro* autoradiography with [11C]**7f** revealed higher accumulation on tissue slices of hCD80-positive Raji than hCD80-negative NCI-H69 xenografts (Supplementary Figures S5 and S6). The binding of [11C]**7f** to hCD80-positive Raji xenograft slices was reduced by an excess of 5 μM **7f**, **1**, **2** and abatacept, respectively, by around 35% of the total binding. No reduction in [11C]**7f** binding was observed with the hCD80-negative tissue slices under these blocking conditions.

In vivo evaluation in Raji xenograft bearing mice. We further evaluated [11C]**7f** *in vivo* by PET/CT imaging. We have recently compared the *in vivo* pharmacokinetics of [11C]**1** and [11C]**7f**

by kinetic modelling with PET data.[19] Both tracers showed low distribution to tissue, in agreement with the high plasma protein binding, but high extraction into the bile relative to the low free fraction in plasma. This resulted in high abdominal radioactivity with spill-over to peripheral tissues in the PET images. The biliary excretion of [^{11}C]**7f** was significantly reduced by pre-administration of cyclosporine, an inhibitor of several hepatic transport proteins.[19] Here, we evaluated the uptake of [^{11}C]**7f** into the Raji xenografts from the data sets which were used for pharmacokinetic modelling in the previous work.[19] Figure 4 shows [^{11}C]**7f** PET images of a Raji xenograft bearing SCID mouse after administration of cyclosporine ~30 min before the tracer. Scarce accumulation of [^{11}C]**7f** in the periphery of the xenograft, as indicated in Figure 4, was observed in two out of four cyclosporine-administered animals. No xenograft accumulation was observed in the four animals without cyclosporine. For comparison, Figure 4 shows in addition a representative [^{18}F]FDG scan of a Raji-xenograft bearing mouse.
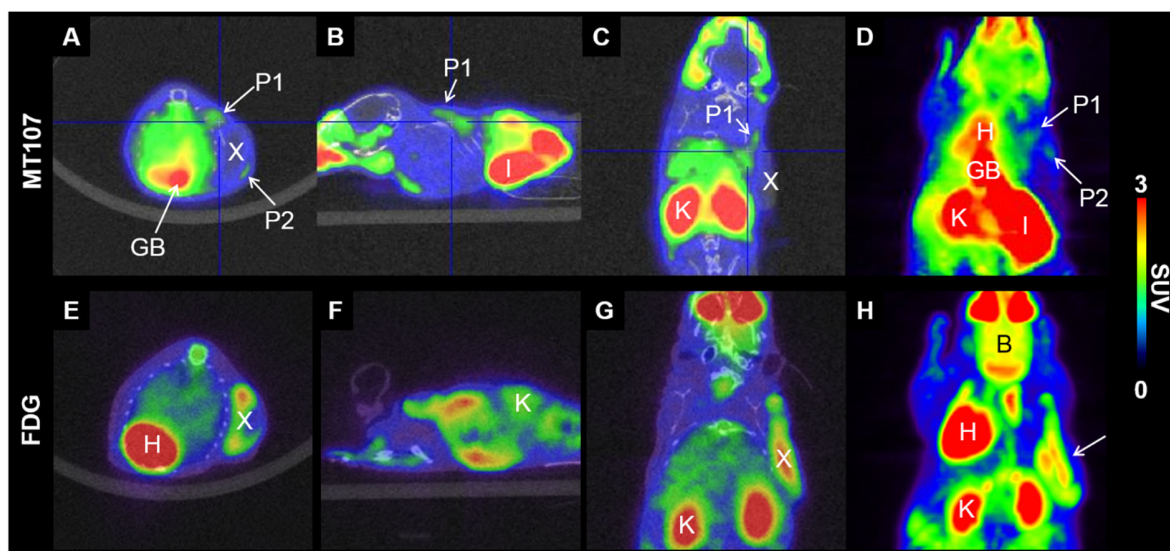

Figure 4: PET/CT images of a Raji (hCD80+) xenograft bearing mouse after tail vein injection of 11.7 MBq (13 nmol/kg) [^{11}C]**7f**, 30 min after i.v. injection of 50 mg/kg cyclosporine (A-D). (E-H)

For comparison, representative PET/CT images of a Raji (hCD80+) xenograft bearing mouse after tail vein injection of 8.6 MBq [^{18}F]FDG. Transversal (A,E), sagittal (B,F) and coronal (C,G) planes, as indicated by the blue cross hairs. (D,H) Maximal intensity projection. CT, grey scale; PET, color scale. H, blood pool (heart); GB, gall bladder; I, intestines; K, kidney; B, brain; P1 and P2, peripheral locations of the xenograft with potential tracer accumulation; X, Raji xenograft. SUV, standardised uptake value. Note that this scan was used for pharmacokinetic modelling in our previous work[19] and that different animals were used for the [^{11}C]**7f** and the [^{18}F]FDG scan.

In order to evaluate the viability of the tumor cells and their general accessibility by radiotracers, additional mice with Raji xenografts were scanned with the glucose analogue [^{18}F]FDG. [^{18}F]FDG uptake was substantial in major parts of the xenografts (Figure 4), confirming the presence of viable tumor tissue. The *in vivo* expression of hCD80 and its localisation on the cell surface were confirmed by flow cytometry and RT-qPCR (Supplementary Figures S7 and S8).

The metabolic stability of [^{11}C]**7f** was investigated in xenograft-free C57BL/6 mice. Only parent tracer was detected in blood plasma, bile and urine 15 min after tracer i.v. injection (Supplementary Figure S9).

DISCUSSION

Our SPR data from a set of novel structures revealed that the methylpiperidine moiety is an essential part for the strong binding to hCD80. Compounds with the N-methyl-piperidine moiety (**1**, **7a**, **7e**, **7f**) showed consistently stronger affinities than compounds with the phenylethan-1-ol moiety. In addition, the cinnoline- and quinoline-based structures showed stronger binding than

17

the pyrazolopyridine-based structures. The modification with an additional CF_3-substituted phenyl ring in position 2 of the quinoline ring system did not affect the binding affinity to hCD80. This suggests that this part of the structure is tolerant for modifications, as was seen for novel structure **7f**, which showed similar affinity as **1** despite an additional bulky group (CF_3 substituted aromatic ring). Taken together, the structure affinity relationship study with hybrid structures of **1** and **2** provides new insights in the structural requirements for CD80 binding and indicates that further modifications are possible without affinity loss.

Displacement of rhCTLA-4 and rhCD28 from hCD80 by **1** and **7f** showed that this low molecular weight compound class has the potential to displace large proteins from binding to hCD80. This ability may be attained by an allosteric mechanism, due to adjacent binding sites on the tertiary structure of hCD80.[13]

The experimental log D at pH 7.4 of [^{11}C]**7f** was two log units higher than that of [^{11}C]**1**. However, lipid bilayer permeation of both compounds **1** and **7f** was poor to moderate. In addition, both had similar high plasma protein binding with a free fraction in plasma of ~ 0.02 (Müller et al.[6] and this study). The free fraction of [^{11}C]**7f** in 4% BSA was ~ 0.15 which indicates that besides albumin an alternative plasma protein may be involved in the binding (assuming binding is similar to human and bovine albumin). This may be α_1-acid glycoprotein, which binds mainly basic compounds.[20]

The negligible uptake of both [^{11}C]**1** and [^{11}C]**7f** into the hCD80-positive xenografts may result from the high plasma protein binding, hampering extravasation of the tracers. The small volume of distribution, in particular of [^{11}C]**7f** (14 % of total body volume[19]) supports this hypothesis. The pre-administration of cyclosporine reduced the biliary excretion significantly and in addition increased the volume of distribution and tissue distribution, though without statistical significance[19]. Both the reduction in spill-over from abdominal radioactivity and potential increase

in tissue distribution may have contributed to the observed increased radioactivity in peripheral parts of the hCD80-rich xenografts in two out of four cyclosporine treated animals.

Biliary excretion as well as strong binding to plasma proteins may depend on the cationic characteristics of the tracers[21,22,23,24]. We currently investigate the effect of the charge and ionization state on the binding affinity to hCD80, biliary excretion, plasma protein binding and finally *in vivo* imaging.

CONCLUSION

A structure-affinity relationship study identified structural features which promote low nanomolar affinity to hCD80. Despite strong *in vitro* binding of **7f** to hCD80, observed by SPR and autoradiography, PET-tracer [^{11}C]**7f** hardly accumulated in hCD80-rich xenografts *in vivo*. High plasma protein binding and high spill-over due to biliary excretion may have hampered observable accumulation. Further structural modifications towards pharmacokinetic optimisation will be based on these results. Besides imaging, our findings may be of interest for the development of therapeutic CD80 inhibitors.

EXPERIMENTAL SECTION

Materials & methods. All chemicals, unless otherwise stated, were purchased from Sigma Aldrich GmbH (Taufkirchen, Germany), ABCR GmbH (Karlsruhe, Germany), Merck (Darmstadt, Germany), Fluorochem Ltd. (Hadfield, GB), Tokyo Chemical Industry Co. Ltd (Tokyo, Japan), Apollo Scientific Ltd (Cheshire, GB) or Fisher Scientific International Inc. (Hampton, US) and were used without further purification.

Solvents for thin layer chromatography (TLC), column chromatography and extractions were commercial grade. Organic chemistry reactions were monitored by TLC using Sigma-Aldrich silica gel 60 plates (UV light at 254 nm). Nuclear magnetic resonance (NMR) spectra (^{1}H and ^{13}C NMR) were obtained on a Bruker Avance FT-NMR spectrometer (400 MHz). Chemical shifts are given in delta (δ) units, in ppm relative to tetramethylsilane (TMS, 0 ppm). Multiplicities in the ^{1}H NMR spectra are described as: s = singlet, d = doublet, t = triplet and m = multiplet. Coupling constants (J) are reported in Hz. High resolution mass spectrometry (HR-MS) was performed by the MS service of the Laboratory for Organic Chemistry at the ETH Zürich. The MALDI spectra were recorded on a Bruker solariX (MALDI-FTICR-MS) or Bruker UltraFlex II (MALDI-TOF-MS), while the ESI were recorded on a Bruker maXis (ESI-Qq-TOF-MS) or Bruker solariX (ESI-FTICR-MS). High-performance liquid chromatography (HPLC) analysis was performed using a reversed phase column (ACE column, C18, 3 μm) with a gradient system of acetonitrile and 50 mM sodium acetate. Semi-preparative HPLC purifications were carried out on a reversed phase column (ACE column, Symmetry C8 5 μm; 7.8 × 50 mm) under following conditions: 4.1 g/L sodium acetate in H$_2$O (solvent A), MeCN (solvent B); isocratic with 25% B; flow rate 4.5 mL/min. The UV signal was measured at a wavelength of 320 nm.

The purity of all biologically tested compounds was ≥ 95%, except of intermediate **6d** with a purity of 92%. Purity was determined by HPLC using an analytical reverse phase column (Xbridge, C18, 5µm; 4.6 x 150mm) with H_2O/MeCN (both containing 0.1% TFA) as mobile phase. Method: 2 min isocratic 5% MeCN followed by a gradient from 5% to 90% MeCN in 12 min. Peaks corresponding to the desired product are described, including retention time (rt) and purity by integration.

The recombinant human CTLA-4 fusion protein abatacept (Orencia®, Bristol-Myers-Squibb) and cyclosporine (Sandimmun®, Novartis) were purchased from a local pharmacy.

All animal experiments were carried out in accordance with the Swiss Animal Welfare legislation and approved by the Veterinary Office of the Canton Zurich (ZH17/2015 and ZH18/2018). Female C.B.17 SCID mice (xenografts) and male C57BL/6 mice (tracer metabolism) were purchased from Charles River Laboratories (Sulzfeld, Germany) and housed under standard conditions (12 h light/12 h dark, free access to chow and water). [^{18}F]FDG was generated in a routine production by the University Hospital Zurich.

Chemistry

4-(6-fluoro-1,3-dihydro-3-oxo-2*H*-pyrazolo[4,3-*c*]cinnolin-2-yl)-*N*-(1-methyl-4-piperidinyl)-benzamide (1). Compound **1** was synthesised from **6b** following the same experimental procedure like the synthesis of 2 and 1-methylpiperidine-4-amine. MS (ESI) calculated for $C_{22}H_{22}FN_6O_2^+$: 421.2; *m/z* found was 421.2 [M+H]$^+$; rt 9.36 min, 95%.

4-[3,6-dihydro-6-methyl-3-oxo-4-[3-(trifluoromethyl)phenyl]dipyrazolo[3,4-*b*:3',4'-*d*]pyridin-2(1*H*)-yl]-*N*-[3-(1-hydroxyethyl)phenyl]-benzamide (2). 100 mg (0.22 mmol) of **6c** were dissolved in 1.1 mL DMF and stirred in a round-bottom flask. 93 mg (0.66 mmol) 1-(3-aminophenyl)ethan-1-ol, 70 μL (0.40 mmol) DIPEA and 85 mg (0.44 mmol) EDC hydrochloride were added and the mixture was stirred for 7 h, before EtOAc and 0.25-M HCl was added, and extraction was performed. The combined organic layers were washed with brine, dried over sodium sulfate, filtered and concentrated. The crude was purified by flash chromatography (9:1 EtOAc:EtOH saturated with ammonium bicarbonate) and relevant fractions were collected and concentrated, which resulted in a product weight of 78 mg (62% yield). HR-MS (ESI) calculated for $C_{30}H_{24}F_3N_6NaO_3^+$: 595.1676; *m/z* found was 595.1675 [M+Na]$^+$; rt 13.58 min, 95%.

2-chloro-5-[3,6-dihydro-6-methyl-3-oxo-4-[3-(trifluoromethyl)phenyl]dipyrazolo[3,4-*b*:3', 4'-*d*]pyridin-2(1*H*)-yl]-benzoic acid (3). 64 mg (0.28 mmol) of 2-chloro-5-hydrazinylbenzoic acid hydrochloride were dispersed in 480 μL ethylene glycol, before 47.4 mg (0.47 mmol) of sodium tert-butoxide were added and the mixture was stirred for 1.5 h at 75°C. It was cooled to rt and 36 mg (0.09 mmol) of **5c** were added with 1 mL of tert-butanol. The mixture was heated at reflux (100°C) for 30 h. After 23 h additional sodium tert-butoxide (85 mg, 0.84 mmol) and another 10 mg (0.05 mmol) of 2-chloro-5-hydrazinylbenzoic acid hydrochloride were added. The reaction was quenched with water and EtOAc. The pH was set to 3 with 0.5-M HCl. The combined organic layers were washed with brine, dried over sodium sulfate, filtered and concentrated. The crude was dissolved in 2-3 mL EtOAc and kept at 0°C for 72 h. Orange precipitation formed, which was filtered and resulted in a product weight of 14.3 mg (31% yield). MS (ESI) calculated for $C_{22}H_{14}ClF_3N_5O_3^+$: 488.1; *m/z* found 488.1 [M+H]$^+$; rt 13.64 min, 95%.

Ethyl-3-methoxy-3-(3-(trifluoromethyl)phenyl)acrylate (4). 5 mL (28 mmol) ethyl 3-(trifluoro-methyl)benzoate were dissolved in 200 mL EtOAc. 1.13 mg (28 mmol) sodium hydride was added under stirring and heated to 40°C for 5 min, before another 1.13 mg (28 mmol) sodium hydride was added and the reaction mixture was heated under reflux (90°C) for 18 h. The reaction was cooled to rt and DCM/water was added. Extraction was performed and the combined organic layers were washed with brine, dried over sodium sulfate, filtered and concentrated. The crude was further dried with benzene under reduced pressure. In a second step, the crude intermediate was dissolved in 100 mL 4:1 MeCN:MeOH and 28 mL (56 mmol) 2-M (diazomethyl)trimethylsilane in hexane was added. The reaction was stirred for 36 h at rt, before it was quenched with 8 mL aqueous 1-M HCl and extraction was performed with EtOAc. The combined organic layers were washed with brine, dried over sodium sulfate, filtered and concentrated, which resulted in 9.63 g crude. Flash chromatography was performed with 95:5 hexane:EtOAc, resulting in a product weight of 3.74 g (48% yield). ^{1}H NMR (400 MHz, Chloroform-d) δ 7.81 (s, 1H), 7.74 (d, J = 7.5 Hz, 1H), 7.68 (d, J = 7.5 Hz, 1H), 7.53 (t, J = 7.5 Hz, 1H), 5.63 (s, 1H), 4.22 (q, J = 7.1 Hz, 2H), 3.90 (s, 3H), 1.31 (t, J = 7.1 Hz, 4H). ^{19}F NMR (376 MHz, Chloroform-d) δ -62.80. HR-MS (ESI) calculated for $C_{13}H_{14}F_3O_3^{+}$: 275.0890; m/z found was 275.0895 $[M+H]^{+}$.

Methyl 4-hydroxylcinnoline-3-carboxylate (5a). To a mixture of 6 mL (84 mmol) thionylchloride and 10 mL chloroform, 4 g (19 mmol) of compound 2-(2-phenylhydrazono)malonic acid was added. The reaction mixture was stirred at 80°C for two hours under nitrogen atmosphere. The solvents were removed under vacuum and the brown residue was re-dissolved in dichloroethane and dried again. The resulting acid chloride was dissolved in 10 mL

dichloroethane, then 1.2 mL TiCl$_4$ were added and the dark brown solution was stirred at 110°C for 4 hours under nitrogen. The reaction mixture was cooled to 10°C, 20 mL methanol were added slowly and the resulting red-brown solution was stirred at 60°C for 30 min. The solvents were removed under reduced pressure and the residues were crystalized from 10 mL acetonitrile to yield 0.6 g of compound **5a** (15% yield). ^{1}H NMR (400 MHz, DMSO-d_6) δ 13.94 (s, 1H), 8.10 (d, J = 8.2 Hz, 1H), 7.84 (t, J = 7.7 Hz, 1H), 7.68 (d, J = 8.2 Hz, 1H), 7.52 (t, J = 7.7 Hz, 1H), 3.83 (s, 3H). MS (ESI) calculated for C$_{10}$H$_9$N$_2$O$_3^+$: 205.1; m/z found was 204.7 [M+H]$^+$.

Methyl 4-hydroxy-8-fluorocinnoline-3-carboxylate (5b). Compound **5b** was synthesized in an analogous way to the procedure for compound **5a**, but with 2-(2-(2-fluorophenyl)hydrazono)malonic acid. ^{1}H NMR (400 MHz, DMSO-d_6) δ 14.19 (s, 1H), 7.90 (d, J = 8.2 Hz, 1H), 7.77 (ddd, J = 11.2, 8.0, 1.2 Hz, 1H), 7.49 (td, J = 8.1, 4.8 Hz, 1H), 3.85 (s, 3H). MS (ESI) calculated for C$_{10}$H$_8$FN$_2$O$_3^+$: 223.0; m/z found was 222.9 [M+H]$^+$.

Ethyl 4-chloro-1-methyl-6-(3-(trifluoromethyl)phenyl)-1*H*-pyrazolo[3,4-*b*]pyridine-5-carboxylate (5c). This intermediate was synthesised from **4** following the same experimental procedure like the synthesis of **5e** and ethyl 5-amino-1-methyl-1H-pyrazole-4-carboxylate, resulting in a product weight of 830 mg (60% yield). ^{1}H NMR (400 MHz, Chloroform-d) δ 8.18 (s, 1H), 7.96 (s, 1H), 7.88 (d, J = 7.8 Hz, 1H), 7.73 (d, J = 7.8 Hz, 1H), 7.60 (t, J = 7.8 Hz, 1H), 4.22 (q, J = 7.1 Hz, 2H), 4.20 (s, 3H), 1.12 (t, J = 7.1 Hz, 3H). MS (ESI) calculated for C$_{17}$H$_{14}$ClF$_3$N$_3$O$_2^+$: 384.1; m/z found was 384.2 [M+H]$^+$.

Ethyl 4-chloro-2-(3-(trifluoromethyl)phenyl)quinoline-3-carboxylate (5d). This intermediate was synthesised from **4** following the same experimental procedure like the synthesis of **5e** and ethyl-2-aminobenzoate, resulting in a product weight of 418 mg (61% yield). ^{1}H NMR (400 MHz, Chloroform-d) δ 8.32 (d, J = 8.4 Hz, 1H), 8.19 (d, J = 8.4 Hz, 1H), 8.03 (s, 1H), 7.95 (d, J = 7.8 Hz, 1H), 7.86 (t, J = 8.4 Hz, 1H), 7.77 – 7.69 (m, 2H), 7.62 (t, J = 7.8 Hz, 1H), 4.29 (q, J = 7.2 Hz, 2H), 1.18 (t, J = 7.2 Hz, 3H). ^{13}C NMR (101 MHz, CDCl$_3$) δ 166.2, 154.7, 148.0, 141.2, 140.0, 132.0, 131.0, 130.1, 129.3, 128.8, 127.1, 126.9, 126.2, 125.6, 125.4, 124.7, 122.7, 62.6, 13.8. ^{19}F NMR (376 MHz, Chloroform-d) δ -62.68. HR-MS (ESI) was calculated for C$_{19}$H$_{13}$ClF$_3$NNaO$_2$$^+$: 380.0660; m/z found was 380.0663 [M+H]$^+$.

Ethyl 4-chloro-8-fluoro-2-(3-(trifluoromethyl)phenyl)quinoline-3-carboxylate (5e). 740 mg (4.4 mmol) of methyl 2-amino-3-fluorobenzoate were dissolved in 8 mL THF, before 193 mg (4.8 mmol) sodium hydride was added and the mixture was stirred at room temperature. After 30 min, 1.20 g (4.4 mmol) of **4** with 1.7 mL THF was transferred to the mixture. The reaction was run under reflux for 16 h, before it was cooled to room temperature and quenched with water. The pH was set to 5 with aqueous HCl. Extraction was performed with EtOAc and the combined organic fractions were dried, filtered and concentrated, which resulted in a crude weight of 1.86 g. The crude was dissolved in 19 mL phosphorus oxychloride and stirred at reflux for 2 h. After cooling to room temperature, it was concentrated under reduced pressure. The residues were dissolved in EtOAc, cooled to 0°C and neutralised with aqueous 5% NaHCO$_3$. Extraction was performed with EtOAc and the collected organic layers were dried over sodium sulfate and concentrated, resulting in a crude weight of 1.81 g. Flash chromatography (9:1 Hexane:EtOAc) was performed, giving a product weight of 955 mg (55% yield). ^{1}H NMR (400 MHz, Chloroform-

d) δ 8.12 (d, J = 8.5 Hz, 1H), 8.02 (s, 1H), 7.98 (d, J = 7.7 Hz, 1H), 7.75 (d, J = 7.7 Hz, 1H), 7.72 – 7.54 (m, 3H), 4.30 (q, J = 7.1 Hz, 1H), 3.84 (s, 2H), 1.19 (t, J = 7.1 Hz, 1H). ^{13}C NMR (101 MHz, CDCl$_3$) δ 165.9, 159.5, 156.9, 154.8, 139.7, 132.2, 129.5, 128.6, 128.5, 128.1, 126.4, 126.3, 125.6, 125.4, 122.7, 120.5, 116.2, 62.8, 13.8. ^{19}F NMR (376 MHz, Chloroform-d) δ -62.66, -122.57. HR-MS (ESI) calculated for $C_{19}H_{13}ClF_4NO_2^+$: 398.0565; m/z found was 398.0565 [M+H]$^+$.

4-(3-oxo-1,3-dihydro-2H-pyrazolo[4,3-c]cinnolin-2-yl)benzoic acid (6a). 0.5 g (2.4 mmol) of compound **5a** were added in 2 mL (27 mmol) thionyl chloride and the reaction mixture was stirred at 80°C for 1 h. The excess of thionyl chloride was removed under vacuum. The residue was dissolved in toluene and the solvent was removed under vacuum to remove the traces of thionyl chloride. Then 0.73 g (4.8 mmol) 4-hydrazinylbenzoic acid and 7 mL ethanol were added and the reaction mixture was stirred at 70°C for 1 h. The resulting precipitates were collected and washed with methanol:37% aqueous HCl mixture (9:1, 10 mL). The crude product was washed additionally 3 times with water, methanol, and methylene chloride and dried to yield 0.57 g of compound **6a** (78% yield). ^{1}H NMR (400 MHz, DMSO-d_6) δ 14.62 (s, 1H), 12.84 (s, 1H), 8.33 (d, J = 8.9 Hz, 2H), 8.21 (d, J = 7.8 Hz, 1H), 8.06 (d, J = 8.9 Hz, 2H), 7.86 – 7.78 (m, 2H), 7.73 – 7.66 (m, 1H). MS (ESI) calculated for $C_{16}H_{11}N_4O_3^+$: 307.1; m/z found was 306.7 [M+H]$^+$; rt 10.78 min, >99%.

4-(6-fluoro-3-oxo-1,3-dihydro-2H-pyrazolo[4,3-c]cinnolin-2-yl)benzoic acid (6b). The structure was synthesised in an analogous way to the procedure of compound **6a** with compound **5b** as starting material. ^{1}H NMR (400 MHz, DMSO-d_6) δ 14.71 (s, 1H), 12.87 (s, 1H), 8.26 (d, J

= 8.9 Hz, 2H), 8.02 (d, J = 8.9 Hz, 2H), 7.96 (d, J = 7.8 Hz, 1H), 7.73 – 7.58 (m, 2H). MS (ESI) calculated for $C_{16}H_{11}FN_4O_3^+$: 325.1; m/z found was 324.7 [M+H]$^+$.

4-(6-methyl-3-oxo-4-(3-(trifluoromethyl)phenyl)-3,6-dihydrodipyrazolo[3,4-b:3',4'-d]pyridin-2(1H)-yl)benzoic acid (6c). This intermediate was synthesised from **5c** following the experimental procedure like the synthesis of **6e**, resulting in a product weight of 825 mg (85% yield). ^{1}H NMR (400 MHz, Acetone-d_6) δ 12.24 (s, 1H), 8.45 (s, 1H), 8.39 (d, J = 7.8 Hz, 1H), 8.22 (s, 1H), 8.12 (s, 4H), 7.87 (d, J = 7.8 Hz, 1H), 7.76 (t, J = 7.8 Hz, 1H), 4.16 (s, 3H). ^{19}F NMR (376 MHz, Acetone-d_6) δ -62.88. HR-MS (ESI) calculated for $C_{22}H_{15}F_3N_5O_3^+$: 454.1122; m/z found was 454.1128 [M+H]$^+$; rt 13.31 min, >99%.

4-(3-oxo-4-(3-(trifluoromethyl)phenyl)-1,3-dihydro-2H-pyrazolo[4,3-c]quinolin-2-yl)benzoic acid (6d). This intermediate was synthesised from **5d** following the same experimental procedure like the synthesis of **6e**, resulting in a product weight of 120 mg (68% yield). ^{1}H NMR (400 MHz, DMSO-d_6) δ 12.72 (s, 1H), 8.39 – 8.32 (m, 3H), 8.30 (d, J = 7.6 Hz, 1H), 8.25 (d, J = 7.8 Hz, 1H), 8.05 (d, J = 7.8 Hz, 1H), 8.01 (d, J = 8.9 Hz, 2H), 7.90 – 7.84 (m, 2H), 7.73 (t, J = 7.6 Hz, 1H), 7.60 (t, J = 7.6 Hz, 1H). ^{13}C NMR (101 MHz, DMSO-d_6) δ 167.5, 162.0, 151.3, 144.7, 143.9, 136.6, 134.7, 131.0, 130.9, 130.7, 129.7, 128.5, 127.4, 127.1, 126.1, 125.8, 123.1, 122.4, 120.3, 118.7 118.2, 102.6. ^{19}F NMR (376 MHz, DMSO-d_6) δ -60.96. MS (ESI) calculated for $C_{24}H_{15}F_3N_3O_3^+$: 450.1; m/z found was 450.1 [M+H]$^+$; rt 13.35 min, 92%.

4-(6-fluoro-3-oxo-4-(3-(trifluoromethyl)phenyl)-1,3-dihydro-2*H*-pyrazolo[4,3-*c*]quinolin-2-yl)benzoic acid (6e). 429 mg (2.82 mmol) of 4-hydrazinylbenzoic acid were dissolved in 4.7 mL ethylene glycol, 279 mg (2.82 mmol) sodium tert-butoxide were added and stirred at 75°C for 1 h. After cooling, 374 mg (0.94 mmol) of **5e** dissolved in 2.0 mL THF were added and the reaction mixture was heated to 100°C. After 16 h, another 100 mg of sodium tert-butoxide was added and stirred at 100°C for another 3 h. The reaction was quenched with H_2O and EtOAc. The crude solution was acidified to pH 3 using 1-M HCl and extracted with EtOAc. The organic layers were dried with sodium sulfate and concentrated, giving 54.4 mg crude. For purification, trituration was performed as described in the synthesis for **7g**. In short, the crude was dissolved in aceton, few 1-M HCl was added and the solution was concentrated at 100 mbar at 40°C until precipitate formed. The suspension was stored in the fridge for 1 h. Filtration, washing with 1-M HCl and cold H_2O, and subsequent drying, resulted in a product weight of 288 mg (66% yield). ^{1}H NMR (400 MHz, DMSO-d_6) δ 12.79 (s, 1H), 12.58 (s, 1H), 8.30 (d, J = 8.9 Hz, 2H), 8.24 (s, 1H), 8.17 (d, J = 7.8 Hz, 1H), 8.08 (d, J = 7.4 Hz, 1H), 8.04 – 7.95 (m, 3H), 7.81 (t, J = 7.8 Hz, 1H), 7.71 – 7.43 (m, 2H). ^{13}C NMR (101 MHz, DMSO-d_6) δ 167.0, 161.3, 153.7, 151.9, 151.2, 143.5, 143.3, 134.6, 130.3, 128.8, 128.5, 128.2, 127.7, 127.2, 126.9 (d, J = 7.6 Hz), 125.7, 125.5, 122.8, 120.4, 117.7, 115.8 (d, J = 17.1 Hz), 103.1.^{19}F NMR (376 MHz, DMSO-d_6) δ -60.92, -124.46. HR-MS (ESI) calculated for $C_{24}H_{14}F_4N_3O_3^+$: 468.0966; *m/z* found was 468.0966 [M+H]$^+$.

N-(1-methylpiperidin-4-yl)-4-(3-oxo-1,3-dihydro-2*H*-pyrazolo[4,3-*c*]cinnolin-2-yl)benzamide (7a). 24.7 mg (0.08 mmol) of **6a** were dissolved in 850 μL 2:1 DCM/THF and 240 μL (3.3 mmol) thionylchloride was added. The mixture was stirred at reflux for 3 h. The reaction was cooled down and solvents were evaporated under reduced pressure. Benzene was

added two times to remove solvent residues, resulting in a crude weight of 32.1 mg. This crude was then resuspended in 200 μL DMF. 12.7 μL (0.10 mmol) 1-methylpiperidin-4-amine and 22.8 μL (0.16 mmol) triethylamine were mixed with 210 μL DMF in a separate flask and then added to the reaction. After 20 hours, the reaction was stopped by adding aqueous HCl solution and EtOAc, which led to the formation of precipitates. The precipitates were washed with aqueous HCl solution and cold water. The precipitates were dissolved with ethanol/water and concentrated to half the volume and stored in the fridge overnight. Orange precipitates formed and were filtered and washed. The precipitates were treated with toluene and dried under high-vacuum to give a final product weight of 6.4 mg (19% yield). ^{1}H NMR (400 MHz, DMSO-d_6) δ 8.35 (d, J = 8.9 Hz, 2H), 8.33 – 8.29 (m, 1H), 8.21 (d, J = 8.0, 1H), 7.97 (d, J = 8.9 Hz, 2H), 7.90 (d, J = 8.0 Hz, 1H), 7.78 (t, J = 7.7 Hz, 1H), 7.66 (t, J = 7.7 Hz, 1H), 3.96 – 3.83 (m, 1H), 3.14 – 3.03 (m, 2H), 2.57 – 2.51 (m, 2H), 2.45 (s, 3H), 1.94 – 1.86 (m, 2H), 1.79 – 1.66 (m, 2H). HR-MS (ESI) calculated for $C_{22}H_{23}N_6O_2^+$: 403.1877; *m/z* found was 403.1875 [M+H]$^+$; rt 9.32 min, 97%.

4-(6-fluoro-3-oxo-1,3-dihydro-2*H*-pyrazolo[4,3-*c*]cinnolin-2-yl)-*N*-(3-(1-hydroxyethyl)phenyl)benzamide (7b). This structure was synthesised from 20 mg of **6b** following the same experimental procedure like the synthesis of **7c**, resulting in a product weight of 11 mg (40% yield). ^{1}H NMR (400 MHz, DMSO-d_6) δ 10.23 (s, 1H), 8.34 (d, J = 8.9 Hz, 2H), 8.13 (d, J = 8.9 Hz, 2H), 8.05 (d, J = 7.6 Hz, 1H), 7.77 (s, 1H), 7.77 (s, 1H), 7.76 – 7.64 (m, 3H), 7.29 (t, J = 7.8 Hz, 1H), 7.08 (d, J = 7.8 Hz, 1H), 5.19 (s, 1H), 4.72 (q, J = 6.5 Hz, 1H), 1.34 (d, J = 6.5 Hz, 3H). ^{19}F NMR (376 MHz, DMSO-d_6) δ -125.47. HR-MS (MALDI/ESI) calculated for $C_{24}H_{18}FN_5NaO_3^+$: 466.1286; *m/z* found was 466.1282 [M+Na]$^+$; rt 11.64 min, 98%.

***N*-(3-(1-hydroxyethyl)phenyl)-4-(3-oxo-1,3-dihydro-2*H*-pyrazolo[4,3-*c*]cinnolin-2-yl)benzamide (7c).** 15 mg (0.05 mmol) of **6a** were dissolved in 600 μL 2:1 DMF/THF and 21 mg (0.15 mmol) of 1-(3-aminophenyl)ethan-1-ol as well as 24 mg (0.12 mmol) 1-ethyl-3-(3-dimethylaminopropyl)carbo-diimid hydrochloride (EDC·HCl) were added. Afterwards, 16 μL (0.09 mmol) DIPEA were added and the reaction was stirred for 16 h at room temperature, before the reaction was quenched by the addition of EtOAc and aqueous 0.25-M HCl. The organic layers were dried over sodium sulfate and concentrated, resulting in a crude weight of 35.1 mg. Flash chromatography (9:1 EtOAc/EtOH, saturated with NH_4HCO_3) was used for purification, which resulted in a product weight of 2.8 mg (13% yield). ^{1}H NMR (400 MHz, Acetone-d_6) δ 9.49 (s, 1H), 8.45 (d, J = 8.9 Hz, 2H), 8.38 (s, 1H), 8.32 (d, J = 7.8 Hz, 1H), 8.21 (d, J = 7.8 Hz, 1H), 8.12 (d, J = 8.9 Hz, 2H), 8.01 (d, J = 7.8 Hz, 1H), 7.92 – 7.81 (m, 2H), 7.79 (d, J = 7.7 Hz, 1H), 7.63 – 7.54 (m, 2H), 7.29 (t, J = 7.7 Hz, 1H), 7.13 (d, J = 7.7 Hz, 1H), 4.85 (q, J = 6.4 Hz, 1H), 4.17 (d, J = 4.1 Hz, 1H), 1.42 (d, J = 6.4 Hz, 3H). HR-MS (ESI) calculated for $C_{24}H_{19}N_5NaO_3^+$: 448.1380; *m/z* found was 448.1386 [M+Na]$^+$; rt 11.53 min, 95%.

4-(6-methyl-3-oxo-4-(3-(trifluoromethyl)phenyl)-3,6-dihydrodipyrazolo[3,4-*b*:3',4'-*d*]pyridin-2(1*H*)-yl)-*N*-(1-methylpiperidin-4-yl)benzamide (7d). This structure was synthesised from 20 mg of **6c** following the same experimental procedure like the synthesis of **7c**, resulting in a product weight of 16 mg (66% yield). ^{1}H NMR (400 MHz, DMSO-d_6) δ 10.62 (s, 1H), 8.59 (d, J = 7.5 Hz, 1H), 8.35 – 8.24 (m, 3H), 8.12 – 7.98 (m, 4H), 7.89 (d, J = 7.8 Hz, 1H), 7.76 (t, J = 7.8 Hz, 1H), 4.11 (s, 3H), 4.08 – 3.97 (m, 1H), 3.46 – 3.42 (m, 3H), 3.15 – 3.01 (m, 2H), 2.79 – 2.68 (m, 2H), 2.07 – 1.90 (m, 4H). ^{19}F NMR (376 MHz, DMSO-d_6) δ -60.88. HR-MS (ESI) calculated for $C_{28}H_{27}F_3N_7O_2^+$: 550.2173; *m/z* found was 550.2167 [M+H]$^+$; rt 11.71 min, 97%.

_N_-(1-methylpiperidin-4-yl)-4-(3-oxo-4-(3-(trifluoromethyl)phenyl)-1,3-dihydro-2_H_-pyrazolo[4,3-_c_]quinolin-2-yl)benzamide (7e). This intermediate was synthesised from **6d** following the same experimental procedure like the synthesis of **7f**, resulting in a product weight of 31 mg (66% yield). ^{1}H NMR (400 MHz, DMSO-d_6) δ 8.40 (s, 1H), 8.39 – 8.30 (m, 3H), 8.28 (d, J = 8.2 Hz, 2H), 7.98 (d, J = 7.8 Hz, 2H), 7.93 (d, J = 8.9 Hz, 2H), 7.87 – 7.77 (m, 2H), 7.66 (t, J = 7.6 Hz, 1H), 7.53 (t, J = 7.6 Hz, 1H), 3.94 – 3.81 (m, 1H), 3.15 – 2.96 (m, 2H), 2.49 – 2.33 (m, 4H), 1.93 – 1.84 (m, 2H), 1.76 – 1.63 (m, 2H). ^{13}C NMR (101 MHz, DMSO-d_6) δ 165.3, 161.3, 152.1, 145.0, 143.7, 142.7, 134.2, 129.7, 129.1, 128.9, 128.7, 128.0, 127.1, 126.7, 125.9, 125.5, 124.2, 121.7, 119.6, 118.9, 117.5, 69.8, 53.7, 45.4, 44.5, 30.3, 29.0. ^{19}F NMR (376 MHz, DMSO-d_6) δ -60.87. HR-MS (ESI) calculated for $C_{30}H_{27}F_3N_5O_2{}^+$: 546.2111; _m/z_ found was 546.2113 [M+H]$^+$; rt 11.53 min, >99%.

4-(6-fluoro-3-oxo-4-(3-(trifluoromethyl)phenyl)-1,3-dihydro-2_H_-pyrazolo[4,3-_c_]quinolin-2-yl)-_N_-(1-methylpiperidin-4-yl)benzamide (7f). 19.4 mg (0.043 mmol) of **6e** were dissolved in 200 µL DMF and stirred in a round-bottom flask. 18.6 mg (0.047 mmol) HATU were added and the mixture was cooled to 0°C. In a separate flask, 16.5 µL (0.13 mmol) 1-methylpiperidin-4-amine and 20 µL (0.13 mmol) DIPEA were mixed with 90 µL DMF and the solution was added dropwise into the reaction mixture at 0°C under vigorous stirring. The reaction was kept stirring for 35 min, before it was quenched by adding 1-M HCl and transferred into an Erlenmeyer tube with ice and brine. This mixture was kept one hour in the fridge and formed precipitates. The suspension was filtered and the precipitates were washed with 1-M HCl. Afterwards, the precipitates were dissolved with EtOH and run through a 0.45 µm filter. The clear yellow solution

was concentrated and dried under high-vacuum, which resulted in a product weight of 20.9 mg (87% yield). For crystal structure check Supplementary Figure S10. ^{1}H NMR (400 MHz, DMSO-d_6) δ 12.62 (s, 1H), 10.52 (s, 1H), 8.52 (d, J = 7.5 Hz, 1H), 8.26 (d, J = 8.9 Hz, 2H), 8.23 (s, 1H), 8.16 (d, J = 7.8 Hz, 1H), 8.13 (d, J = 7.6 Hz, 0H), 8.02 (d, J = 7.8 Hz, 1H), 7.97 (d, J = 8.9 Hz, 2H), 7.83 (t, J = 7.8 Hz, 1H), 7.70 – 7.55 (m, 2H), 4.09 – 3.97 (m, 1H), 3.50 (s, 3H), 3.44 – 3.36 (m, 2H), 3.16 – 2.99 (m, 2H), 2.07 – 1.86 (m, 4H). ^{19}F NMR (376 MHz, DMSO-d_6) δ -60.91, -124.48. HR-MS (MALDI/ESI) calculated for $C_{30}H_{26}F_4N_5O_2^+$: 564.2017; m/z found was 564.2016 [M+H]$^+$; rt 11.72 min, 97%.

4-(6-fluoro-3-oxo-4-(3-(trifluoromethyl)phenyl)-1,3-dihydro-2H-pyrazolo[4,3-c]quinolin-2-yl)-N-(3-(1-hydroxyethyl)phenyl)benzamide (7g). 17.6 mg (0.04 mmol) of **6e** were dissolved in 190 μL DMF and stirred in a round-bottom flask. 16.2 mg (0.12 mmol) 1-(3-aminophenyl)ethan-1-ol, 14.9 mg (0.08 mmol) EDC·HCl and 12 μL (0.07 mmol) DIPEA was added in this respective order. The reaction mixture was stirred at room temperature for 18 h, before it was diluted with EtOAc. The organic layers were partitioned with 0.4-M HCl, dried and concentrated. The crude was dissolved in 5 mL Aceton and 0.5 mL 1-M HCl were subsequently added. The solution was concentrated at 100 mbar at 40°C until red-orange precipitate formed and was stored in the fridge for 1 h. Afterwards the suspension was filtered and the precipitates were washed with 1-M HCl and cold H_2O. The precipitates were dissolved with 9:1 EtOAc:EtOH. The solution was concentrated and dried under high-vacuum, which resulted in a product weight of 5.5 mg (25% yield). ^{1}H NMR (400 MHz, Acetone-d_6) δ 9.49 (s, 1H), 8.45 (d, J = 9.0 Hz, 2H), 8.38 (s, 1H), 8.32 (d, J = 7.9 Hz, 1H), 8.21 (dt, J = 7.8, 1.3 Hz, 1H), 8.12 (d, J = 9.0 Hz, 2H), 8.01 (d, J = 8.0 Hz, 1H), 7.88 – 7.77 (m, 3H), 7.63 – 7.54 (m, 2H), 7.29 (t, J = 7.8 Hz, 1H), 7.13 (d, J = 7.8 Hz, 1H),

4.85 (q, J = 6.1 Hz, 1H), 4.17 (d, J = 4.0 Hz, 1H), 1.42 (d, J = 6.4 Hz, 3H). ^{19}F NMR (376 MHz, Acetone-d_6) δ -63.05, -129.05. HR-MS (ESI) calculated for $C_{32}H_{22}F_4N_4NaO_3^+$: 609.1520; m/z found was 609.1519 [M+Na]$^+$; rt 13.91 min, 98%.

4-(6-fluoro-3-oxo-1,3-dihydro-2H-pyrazolo[4,3-c]cinnolin-2-yl)-N-(piperidin-4-yl)benzamide (8a). Compound **8a** was synthesised from **6b** following the same experimental procedure like the synthesis of **8b** and as described in the supplementary part of a previous publication.[6]
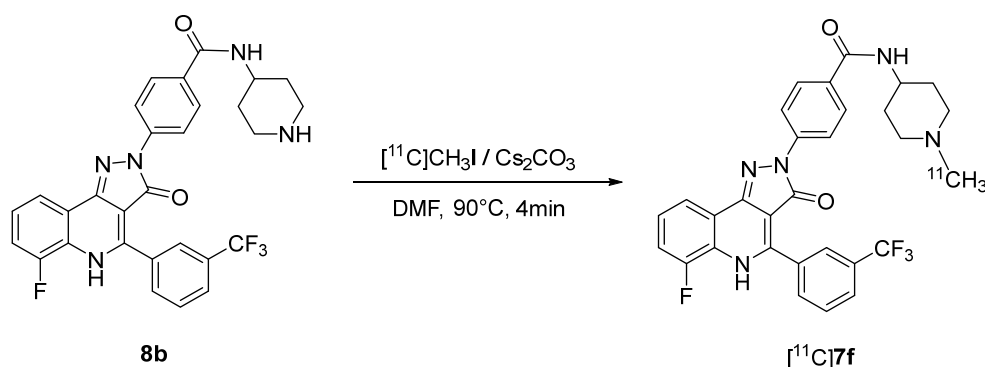
4-(6-fluoro-3-oxo-4-(3-(trifluoromethyl)phenyl)-1,3-dihydro-2H-pyrazolo[4,3-c]quinolin-2-yl)-N-(piperidin-4-yl)benzamide (8b). 16 mg (0.034 mmol) of **6e** were dissolved in 350 μL 2:1 DMF/THF. Afterwards, 8.0 mg (0.041 mmol) EDC·HCl, 41 μL (0.041 mmol) HOBt, 30 μL (0.171 mmol) DIPEA and 17.1 mg (0.086 mmol) tert-butyl 4-aminopiperidine-1-carboxylate were added in this respective order. The reaction was run for 22.5 h at room temperature. The mixture was quenched with EtOAc and H$_2$O, and partitioned. The organic layers were dried over sodium sulfate and concentrated, resulting in a crude weight of 51.1 mg. Flash chromatography (1:1 Hexane:EtOAc + 0.5% Acetic Acid) was performed for purification. After drying the product three times with toluene, the weight of the intermediate was 20.1 mg. The intermediate was then dissolved and stirred in DCM with 20% TFA for 1 h before concentrating under reduced pressure. DCM and acidified water was added and an extraction was performed once. The water phase was neutralised with aqueous 25% NH$_3$ solution and extraction with EtOAc was performed (5x). After concentration under reduced pressure, this resulted in a product weight of 10.7 mg (70% yield).

^{1}H NMR (400 MHz, Methanol-d_4) δ 8.22 (s, 1H), 8.17 (d, J = 8.9 Hz, 2H), 8.13 (d, J = 7.8 Hz, 1H), 8.11 – 8.08 (m, 1H), 7.96 (d, J = 7.8 Hz, 1H), 7.85 (d, J = 8.9 Hz, 2H), 7.79 (t, J = 7.8 Hz, 1H), 7.54 – 7.47 (m, 1H), 7.46 – 7.38 (m, 1H), 4.21 – 4.11 (m, 1H), 3.52 – 3.44 (m, 2H), 3.20 – 3.10 (m, 2H), 2.25 – 2.16 (m, 2H), 1.94 – 1.82 (m, 2H). ^{13}C NMR (101 MHz, Methanol-d_4) δ 169.2, 163.2, 155.2, 153.6, 152.7, 145.0, 143.6, 138.9, 135.1, 131.6, 131.2, 130.2, 129.9, 129.2, 128.2, 126.3, 121.9, 120.4, 119.2, 116.8, 116.6, 46.4, 44.4, 29.5. ^{19}F NMR (376 MHz, Methanol-d_4) δ -63.92, -128.25. HR-MS (MADLI/ESI) calculated for $C_{29}H_{24}F_4N_5O_2^+$: 550.1861; *m/z* found was 550.1861 [M+H]$^+$.

Radiosynthesis of [^{11}C]1 and [^{11}C]7f. The radiotracers were synthesized as shown in Scheme 4 and as recently described for [^{11}C]1, with slight modifications.[6] [^{11}C]CO$_2$ was produced by proton bombardment of nitrogen gas fortified with 0.5% oxygen in a Cyclone 18/9 cyclotron (18-MeV; IBA, Ottignies-Louvain-la-Neuve, Belgium) via the ^{14}N(p,a)^{11}C nuclear reaction. In a first step, nickel-based catalytic reduction of [^{11}C]CO$_2$ yielded [^{11}C]methane which was subsequently iodinated to give [^{11}C]MeI. The [^{11}C]MeI was bubbled into a solution of 1.0 mg precursor (**8a** for [^{11}C]1 and **8b** for [^{11}C]7f, respectively) in 0.6 mL DMF and 5 mg cesium carbonate. The mixture was stirred at 90°C for 4 min. After dilution of the reaction with 1.6 mL 50 mM sodium acetate, the crude solution was purified by semi-preparative HPLC. The radiotracer was collected into 10 mL water and passed through a C18 cartridge. After washing with 5 mL water, the radiotracer was eluted with 0.5 mL ethanol into a sterile vial and diluted with 9.5 mL sterile 0.9% NaCl solution. For quality control, 100 µL of the final formulation was injected into the analytical HPLC system. Identity of the product was confirmed by comparison with the retention time of the

standard reference. The molar activity was calculated from the linear regression of a UV-intensity based calibration curve of the cold reference.

Scheme 4. Radiosynthesis of [^{11}C]**7f** from precursor **8b**.

8b   [^{11}C]**7f**

Radiosynthesis of [^{11}C]7f. Radiotracer [^{11}C]**7f** was prepared with precursor (**8b**) according to the above described radiosynthetic strategy of [^{11}C]**1**.[6]

Lipophilicity and lipid bilayer permeability. [^{11}C]**7f** (6 MBq in 20 µl) was mixed for 30 min in triplicates with 0.5 mL PBS-saturated 1-octanol and 0.5 mL PBS adjusted to pH 5.4, 7.4, 9.0 and 11.0, respectively. After centrifugation, 100 µL of each phase was measured in a gammacounter (Wizard, PerkinElmer) and log D was calculated as the logarithmic ratio between the 1-octanol and buffer phase. The data was analysed by non-linear regression with Equation 1:

$$D = \frac{P_i}{1+10^{(pK_a-pH)}} + \frac{P_n}{1+10^{(pH-pK_a)}} \qquad \text{Eq. 1}$$

where P_i and P_n are the lower and upper plateaux of the function, *i.e.*, P of the ionised and neutral species, respectively. The log P corresponds to the logarithmic P_n.

Lipid bilayer permeability (P_{FLipP}) was determined according to Hermann *et al.*[18] with unilamellar 1-palmitoyl-2-oleoyl-*sn*-glycero-3-phosphocholine liposomes in 20 mM 3-morpholinopropane-sulfonic acid/190 mM NaCl at pH 7.4.

SPR affinity and displacement assays. The SPR affinity assay was performed using a high capacity amine chip with a dextran surface, which was activated using 1-ethyl-3-(3-dimethylaminopropyl)carbodiimid and *N*-hydroxysuccinimid (EDC/NHS) and subsequently coated with recombinant human CD80. The protein coated chip was kept under a steady flow of running buffer (25 mM Tris, 150 mM NaCl, pH 7.2, containing 0.01% TWEEN® 20 and 5% DMSO). The analytes were diluted with running buffer from a micromolar to a subnanomolar concentration range. For the measurement, 100 µL of each dilution was injected with an injection rate of 25 µL/min.

The SPR displacement assay was performed using an amine chip with a dextran surface, which was activated using EDC/NHS and subsequently coated with rhCD80, rmCD80 or rhCD86. The protein coated chip was kept under a steady flow of running buffer. The analytes were diluted with 2 nM rhCTLA-4 or 50 nM rhCD28 solutions in running buffer (25 mM Tris, 150 mM NaCl, pH 7.2, containing 0.01% TWEEN® 20 and 2.5% DMSO), from a micromolar to a subnanomolar concentration range. For the measurement, 100 µL of each dilution was injected with an injection rate of 25 µL/min.

All SPR experiments were carried out on a Sierra SPR-2 device (Sierra Sensors, Hamburg, Germany). Data were analysed with the software Sierra Analyser (version 3.1.10.0). The Scrubber software (version 2.0c, BioLogic Software, Canberra, Australia) revealed similar results (data not

shown). K_i values were estimated from the IC$_{50}$ value, the K_d and the concentration of the displaced ligand, according to the Cheng-Prusoff equation.[25]

Plasma protein binding. For the evaluation of plasma protein binding, 0.5-1 MBq radiotracer was added per 150 µL plasma. The samples were incubated at room temperature for 10 min. To each 150 µL radiotracer-plasma solution was added 300 µL ice-cold PBS and all samples were briefly vortexed. The samples were centrifuged at 14'000 x g in Amicon® Centrifugal Filters with a size cutoff of 10 kDa for 15 min at 4°C. The filters were then inverted and briefly centrifuged at 200 x g for 3 min to obtain the protein fraction. The radioactivity in Becquerel of the protein fraction (A_{protein}), filtrate and filter unit were measured in a gammacounter (Wizard, PerkinElmer), A_{total} was calculated as the sum of these radioactivities, and the free fraction f_u was calculated according to equation 2:

$$f_{\text{u}} = 1 - \frac{A_{\text{protein}}}{A_{\text{total}}} \qquad \text{Eq. 2}$$

Animal xenograft model and PET/CT. Raji cells (DSMZ, Braunschweig, Germany) were cultured according to the supplier's recommendation. For inoculations, 2×10^6 Raji cells were mixed with 100 µL Matrigel (Corning Inc, US) and subcutaneously injected in the right shoulder of SCID mice. PET/CT scans were performed 10 to 15 days after inoculation when the tumor volume was between 1.25 and 1.76 cm^3. For PET/CT imaging, mice were anesthetized by inhalation of 2-5% isoflurane. Respiratory rate and body temperature were controlled as described elsewhere.[6] [^{11}C]**7f** (5-12 MBq, 13-19 nmol/kg) was injected intravenously into the tail vein and a

dynamic PET scan was run from 1 to 61 min post-injection with a subsequent CT scan, both on a Super Argus PET/CT (Sedecal S.A., Madrid, Spain). Note that the same data sets were used in our previous publication where details on data reconstruction are available.[19] The reconstructed PET/CT data were analysed using PMOD software (PMOD, Zurich, Switzerland; version 3.8). Tissue radioactivity was expressed as standardized uptake values (SUV), which is the decay-corrected image-derived radioactivity per cm^3 tissue (multiplied with 1 g/cm^3), divided by the injected radioactivity dose per gram of body weight.

In vivo metabolism of [^{11}C]7f. [^{11}C]7f (55-74 MBq) was injected intravenously in three 15-16 weeks old male C57BL/6 mice. The mice were decapitated under isoflurane anaesthesia 15 min (2 animals) and 60 min (1 animal) after tracer injection and blood, bile and urine were collected. Plasma was separated by centrifugation (1000 x g for 5 min at 4°C) and proteins were denatured with an equal volume of MeCN on ice. After precipitation of the denatured proteins by centrifugation, the filtrated supernatants were analysed by UHPLC. Bile and urine were mixed with equal volumes of MeCN and filtrated for analysis by UHPLC. At 60 min post injection the signal-to-noise ratio in plasma and urine were too low for evaluation.

Single-crystal X-ray diffraction. Structure was refined with SHELXL-2018/3 and SHELXLE.[26,27] Figure S10 was created with PLATON.[28] Data were collected at beamline PXI at the Swiss Light Source, PSI. See CIF file for further details. CIF file deposited with CCDC number 1937859.

Statistical analysis. Data were statistically evaluated with student's t test and non-linear curve fitting with GraphPad Prism Software (Version 7.02, GraphPad Software Inc.) for IC50 or Excel Solver (Microsoft Office 2016) for log D.

ANCILLARY INFORMATION

Supporting Information Availability

The Supporting Information is available free of charge on the ACS Publications website at

http://pubs.acs.org.

- Molecular formula strings (CSV)
- Supporting material (PDF) containing:
    - [S1] SPR sensorgrams of the binding of **1** and **7f** to hCD80
    - [S2] SPR displacement of abatacept by compound **7f** on hCD86
    - [S3] SPR displacement of abatacept by compound **7f** on mCD80
    - [S4] pH-Dependent distribution of [^{11}C]**7f** between 1-octanol and PBS
    - [S5] Autoradiography with hCD80-positive & -negative xenograft slices with [^{11}C]**7f**
    - [S6] Quantification of autoradiographic experiment with [^{11}C]**7f**
    - [S7] Cell surface expression of hCD80, hCD86 and hCTLA-4 by flow cytometry
    - [S8] mRNA expression levels of hCD80/hCTLA-4/hCD28 in Raji and NCI xenografts
    - [S9] UHPLC chromatograms of *in vivo* samples from mice 15 min after [^{11}C]**7f** injection
    - [S10] Crystal data and structure refinement for compound **7f**

Corresponding Authors Information

Marco F. Taddio: marco.taddio@alumni.ethz.ch

Stefanie D. Krämer: stefanie.kraemer@pharma.ethz.ch

Abbrebiations used

Bq, becquerel; CT, computed tomography; CTLA-4, cytotoxic T-lymphocyte-associated protein 4; DIPEA, *N,N*-diisopropylethylamine; EDC, 1-ethyl-3-(3-dimethylaminopropyl)carbodiimide; EtOAc, ethyl acetate; EtOH, ethanol; FDG, fludeoxyglucose; HATU, 1-[bis(dimethylamino)methylene]-1H-1,2,3-triazolo[4,5-b]pyridinium 3-oxid hexafluorophosphate; HR-MS, high resolution mass spectrometry; HOBt, hydroxybenzotriazole; K_d, dissociation constant; kDa, kilodalton; MeCN, acetonitrile; MeOH, methanol; NHS, *N*-hydroxysuccinimide; RT-qPCR, real-time polymerase chain reaction; SPR, surface plasmon resonance; SUV, standardized uptake value.

REFERENCES

(1)   Tivol, E. A.; Borriello, F.; Schweitzer, A. N.; Lynch, W. P.; Bluestone, J. A.; Sharpe, A. H. Loss of CTLA-4 Leads to Massive Lymphoproliferation and Fatal Multiorgan Tissue Destruction, Revealing a Critical Negative Regulatory Role of CTLA-4. *Immunity* **1995**, *3* (5), 541–547. https://doi.org/10.1016/1074-7613(95)90125-6.

(2)   Chen, L.; Flies, D. B. Molecular Mechanisms of T Cell Co-Stimulation and Co-Inhibition. *Nature Reviews Immunology*. 2013, pp 227–242. https://doi.org/10.1038/nri3405.

(3)   Schietinger, A.; Greenberg, P. D. Tolerance and Exhaustion: Defining Mechanisms of T Cell Dysfunction. *Trends in Immunology*. 2014, pp 51–60. https://doi.org/10.1016/j.it.2013.10.001.

(4)   Seliger, B.; Marincola, F. M.; Ferrone, S.; Abken, H. The Complex Role of B7 Molecules in Tumor Immunology. *Trends in Molecular Medicine*. 2008, pp 550–559. https://doi.org/10.1016/j.molmed.2008.09.010.

(5)   Dietel, B.; Altendorf, R.; Cicha, I.; Garlichs, C. Migration of Regulatory T Cells into Human Atherosclerotic Lesions Is Associated with Plaque Stability and Correlates Inversely with Infiltrated Mature Dendritic Cells. *Eur. Heart J.* **2013**, *34*, 441.

(6)   Müller, A.; Mu, L.; Meletta, R.; Beck, K.; Rancic, Z.; Drandarov, K.; Kaufmann, P. A.; Ametamey, S. M.; Schibli, R.; Borel, N.; Krämer, S. D. Towards Non-Invasive Imaging of Vulnerable Atherosclerotic Plaques by Targeting Co-Stimulatory Molecules. *Int. J. Cardiol.* **2014**, *174* (3), 503–515. https://doi.org/10.1016/j.ijcard.2014.04.071.

(7)   Adams, A. B.; Ford, M. L.; Larsen, C. P. Costimulation Blockade in Autoimmunity

Costimulation Blockade in Autoimmunity and Transplantation: The CD28 Pathway. *J Immunol* **2016**, *197* (6), 2045–2050. https://doi.org/10.4049/jimmunol.1601135.

(8)   Biancone, L.; Segoloni, G.; Turello, E.; Donati, D.; Bussolati, B.; Piccoli, G.; Camussi, G. Expression of Inducible Lymphocyte Costimulatory Molecules in Human Renal Allograft. *Nephrol. Dial. Transplant* **1998**, *13* (3), 716–722.

(9)   Kremer, J. M.; Westhovens, R.; Leon, M.; Di Giorgio, E.; Alten, R.; Steinfeld, S.; Russell, A.; Dougados, M.; Emery, P.; Nuamah, I. F.; Williams, G. R.; Becker, J. C.; Hagerty, D. T.; Moreland, L. W. Treatment of Rheumatoid Arthritis by Selective Inhibition of T-Cell Activation with Fusion Protein CTLA4Ig. *N. Engl. J. Med.* **2003**, *349* (20), 1907–1915. https://doi.org/10.1056/nejmoa035075.

(10)   Cutolo, M.; Nadler, S. G. Advances in CTLA-4-Ig-Mediated Modulation of Inflammatory Cell and Immune Response Activation in Rheumatoid Arthritis. *Autoimmunity Reviews*. 2013, pp 758–767. https://doi.org/10.1016/j.autrev.2013.01.001.

(11)   Larsen, C. P.; Pearson, T. C.; Adams, A. B.; Tso, P.; Shirasugi, N.; Strobert, E.; Anderson, D.; Cowan, S.; Price, K.; Naemura, J.; Emswiler, J.; Greene, J.; Turk, L. A.; Bajorath, J.; Townsend, R.; Hagerty, D.; Linsley, P. S.; Peach, R. J. Rational Development of LEA29Y (Belatacept), a High-Affinity Variant of CTLA4-Ig with Potent Immunosuppressive Properties. *Am. J. Transplant.* **2005**, *5* (3), 443–453. https://doi.org/10.1111/j.1600-6143.2005.00749.x.

(12)   Rostaing, L.; Vincenti, F.; Grinyõ, J.; Rice, K. M.; Bresnahan, B.; Steinberg, S.; Gang, S.; Gaite, L. E.; Moal, M. C.; Mondragõn-Ramirez, G. A.; Kothari, J.; Pupim, L.; Larsen, C. P. Long-Term Belatacept Exposure Maintains Efficacy and Safety at 5 Years: Results from the Long-Term Extension of the BENEFIT Study. *Am. J. Transplant.* **2013**, *13* (11), 2875–2883.

https://doi.org/10.1111/ajt.12460.

(13)   Erbe, D. V.; Wang, S.; Xing, Y.; Tobin, J. F. Small Molecule Ligands Define a Binding Site on the Immune Regulatory Protein B7.1. *J. Biol. Chem.* **2002**, *277* (9), 7363–7368. https://doi.org/10.1074/jbc.M110162200.

(14)   Green, N. J.; Xiang, J.; Chen, J.; Chen, L.; Davies, A. M.; Erbe, D.; Tam, S.; Tobin, J. F. Structure-Activity Studies of a Series of dipyrazolo[3,4-b:3',4'-d]pyridin-3-Ones Binding to the Immune Regulatory Protein B7.1. *Bioorganic Med. Chem.* **2003**, *11* (13), 2991–3013. https://doi.org/10.1016/S0968-0896(03)00183-4.

(15)   Huxley, P.; Sutton, D. H.; Debnam, P.; Matthews, I. R.; Brewer, J. E.; Rose, J.; Trickett, M.; Williams, D. D.; Andersen, T. B.; Classon, B. J. High-Affinity Small Molecule Inhibitors of T Cell Costimulation: Compounds for Immunotherapy. *Chem. Biol.* **2004**, *11* (12), 1651–1658. https://doi.org/10.1016/j.chembiol.2004.09.011.

(16)   Uvebrant, K.; Da, D.; Thrige, G.; Rosén, A.; Åkesson, M.; Berg, H.; Walse, B.; Björk, P. Discovery of Selective Small-Molecule CD80 Inhibitors. *J. Biomol. Screen.* **2007**, *12* (4), 464–472. https://doi.org/10.1177/1087057107300464.

(17)   Li, K.; Cheng, X.; Tilevik, A.; Davis, S. J.; Zhu, C. In Situ and in Silico Kinetic Analyses of Programmed Cell Death-1 (PD-1) Receptor, Programmed Cell Death Ligands, and B7-1 Protein Interaction Network. *J. Biol. Chem.* **2017**, *292* (16), 6799–6809. https://doi.org/10.1074/jbc.M116.763888.

(18)   Hermann, K. F.; Neuhaus, C. S.; Micallef, V.; Wagner, B.; Hatibovic, M.; Aschmann, H. E.; Paech, F.; Alvarez-Sanchez, R.; Krämer, S. D.; Belli, S. Kinetics of Lipid Bilayer Permeation

of a Series of Ionisable Drugs and Their Correlation with Human Transporter-Independent Intestinal Permeability. *Eur. J. Pharm. Sci.* **2017**, *104*, 150–161. https://doi.org/10.1016/j.ejps.2017.03.040.

(19)   Taddio, M. F.; Mu, L.; Keller, C.; Schibli, R.; Krämer, S. D. Physiologically Based Pharmacokinetic Modelling with Dynamic PET Data to Study the in Vivo Effects of Transporter Inhibition on Hepatobiliary Clearance in Mice. *Contrast Media Mol. Imaging* **2018**, Article ID 5849047. https://doi.org/10.1155/2018/5849047.

(20)   Paxton, J. W. Alpha1-Acid Glycoprotein and Binding of Basic Drugs. *Methods and Findings in Experimental and Clinical Pharmacology*. 1983, pp 635–648.

(21)   Neef, C.; Meijer, D. K. F. Structure-Pharmacokinetics Relationship of Quaternary Ammonium Compounds. *Naunyn. Schmiedebergs. Arch. Pharmacol.* **2004**, *328* (2), 111–118. https://doi.org/10.1007/bf00512059.

(22)   Jonker, J. W.; Wagenaar, E.; Mol, C. A. A. M.; Buitelaar, M.; Koepsell, H.; Smit, J. W.; Schinkel, A. H. Reduced Hepatic Uptake and Intestinal Excretion of Organic Cations in Mice with a Targeted Disruption of the Organic Cation Transporter 1 (Oct1 [Slc22a1]) Gene. *Mol. Cell. Biol.* **2001**, *21* (16), 5471–5477. https://doi.org/10.1128/MCB.21.16.5471.

(23)   Urien, S.; Tillement, J.-P. pH-Dependency of Basic Ligand Binding to alpha1-Acid Glycoprotein (Orosomucoid). *Biochem. J.* **1991**, *280*, 277–280. https://doi.org/10.1042/bj2800277.

(24)   Huang, Z.; Ung, T. Effect of Alpha-1-Acid Glycoprotein Binding on Pharmacokinetics and Pharmacodynamics. *Curr. Drug Metab.* **2013**, *14* (2), 226–238.

(25)   Yung-Chi, C.; Prusoff, W. H. Relationship between the Inhibition Constant (KI) and the Concentration of Inhibitor Which Causes 50 per Cent Inhibition (I50) of an Enzymatic Reaction. *Biochem. Pharmacol.* **1973**, *22* (23), 3099–3108. https://doi.org/10.1016/0006-2952(73)90196-2.

(26)   Sheldrick, G. M. Crystal Structure Refinement with SHELXL. *Acta Crystallogr. Sect. C Struct. Chem.* **2015**, *71*, 3–8. https://doi.org/10.1107/S2053229614024218.

(27)   Hübschle, C. B.; Sheldrick, G. M.; Dittrich, B. ShelXle: A Qt Graphical User Interface for SHELXL. *J. Appl. Crystallogr.* **2011**, *44* (6), 1281–1284. https://doi.org/10.1107/S0021889811043202.

(28)   Spek, A. L. PLATON SQUEEZE: A Tool for the Calculation of the Disordered Solvent Contribution to the Calculated Structure Factors. *Acta Crystallogr. Sect. C Struct. Chem.* **2015**, *71*, 9–18. https://doi.org/10.1107/S2053229614024929.